

Article

Ni-Cu Alloyed Austempered Ductile Iron Resistance to Multifactorial Wear

Andrzej Norbert Wiczorek 

Faculty of Mining, Safety Engineering and Industrial Automation, Silesian University of Technology, Akademicka 2 Street, 44-100 Gliwice, Poland; andrzej.n.wiczorek@polsl.pl; Tel.: +48-32-237-15-84

Abstract: The paper provides a discussion on the results of studies of the effect exerted by combined degradation factors typical of four types of wear: abrasion, impact–abrasion, tribocorrosion, and impact–abrasion–corrosion, conducted for chain wheels made of Ni-Cu alloyed austempered ductile iron. The studies consisted of determining the content of retained austenite in the structure of the cast irons in question, establishing the measures of wear following wear testing, and identifying the basic surface degradation mechanisms observed in the chain wheels tested following multifactorial wear processes. The chain wheels made of ADI were found to have sustained the greatest damage under the impact–abrasion–corrosion (three-factor) wear scenario, while the wear was least advanced in the abrasion (one-factor) wear case. Another observation derived from the studies is that the combined effect of dynamic forces, corrosion, and quartz sand-based abrasives causes increased surface degradation in the cast iron grades taken into consideration compared to processes characterised by a reduced number of degradation factors (i.e., one- or two-factor wear processes). Additional hardness tests and XRD analyses revealed that a distinctive effect attributable to combined degradation factors on the surface hardness increased value and implied that bench testing was followed by phase transition.

Keywords: mining; wear; scraper conveyors; austempered ductile iron



Citation: Wiczorek, A.N. Ni-Cu Alloyed Austempered Ductile Iron Resistance to Multifactorial Wear. *Lubricants* **2024**, *12*, 131. <https://doi.org/10.3390/lubricants12040131>

Received: 16 February 2024

Revised: 6 April 2024

Accepted: 9 April 2024

Published: 15 April 2024



Copyright: © 2024 by the author. Licensee MDPI, Basel, Switzerland. This article is an open access article distributed under the terms and conditions of the Creative Commons Attribution (CC BY) license (<https://creativecommons.org/licenses/by/4.0/>).

1. Introduction

In the course of machinery operation [1–3], the working environment can exert a multifactorial effect. The foregoing results from the potential occurrence of degradation promote factors [4–7] such as the following:

- Hard abrasives in the zone of the mating of machine components, which intensify abrasive processes;
- Saline waters, which tend to induce electrochemical corrosion processes;
- Dynamic excitations caused by start-up operations or sudden load changes which, in turn, can cause cracks in the microstructure, leading to material decohesion.

A coincidence of at least two of the aforementioned degradation factors is decisive of the complex form of the damage mechanisms observed in machine components; for instance, micro-scratching or micro-ridging, typical of abrasive wear, can be accompanied by surface layer cracking.

The combined effect of dynamic forces and abrasive material [8–10] is typically referred to as impact–abrasion wear, which occurs in the operation of mining machinery (e.g., crushers, skips, and chutes). The resultant effect of both environmental factors should cause a significant wear increase, exceeding the sum of individual effects these factors trigger. This assumption has been confirmed in numerous papers, including by Kennedy et al. [11] who addressed the impact–abrasion wear tests performed on coated and non-coated samples of aluminium, mild steel, and tool steel using a dedicated test rig. The experimental tests they conducted revealed higher wear rates under impact–abrasion conditions compared to

contact-only abrasion. Similar insights have been formulated with reference to studies of diverse materials in papers [12–19].

The wear process triggered by the combined effect of the factors which intensify abrasive and corrosive wear is known as tribocorrosion [20–23]. Under such conditions, the friction-induced wear process and electrochemical corrosion interact, while the consequence of both these processes acting together is a synergy of degradation factors. The synergistic effect observed in the course of the tribocorrosion process is attributable to the removal of the oxide layer due to friction, which accelerates surface corrosion in areas exposed by the impact of the abrasive material or peaks of surface irregularities, while on the other hand, the hard particles of the oxide layers being removed can intensify deterioration of the surface layer [24–26]. The evolution of tribocorrosion-induced damage is schematically shown in Figure 1. Both the process of tribocorrosion and its effects have been described in numerous papers, including [27–33].

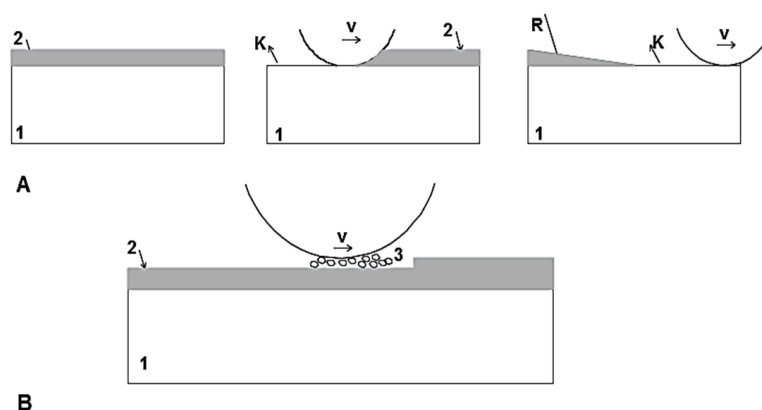


Figure 1. Schematic representation of the tribocorrosion wear mechanism: (A) intensification of the corrosion process due to friction; (B) intensification of the wear process due to the action of oxide layer particles. Designations: 1—base material, 2—oxide layer, 3—comminuted oxide layer fragments, R—repassivation, K—corrosion, v—sliding velocity; based on [23].

Contemporary ADIs are used relatively frequently in the mining industry where machine components are exposed to abrasive wear. They offer a number of advantages which make them suitable as a material for machine parts [34,35], including the following:

- Possibility of using casting technologies to manufacture components from ADI [36–39];
- High mechanical strength of the ADI grades [40–42];
- Possibility of shaping the properties of ADI by way of dedicated heat treatment [43–46] and surface treatment [47–50];
- Possibility of developing a nanocrystalline structure [51–55];
- Option of cast iron surface hardening in processes such as TRIP [56–61] and capacity to attain high tribological wear resistance [62–68].

Even though there are numerous studies on the properties of ausferritic cast irons, few of them have actually addressed the combined effect of numerous degradation factors (impact–abrasion and tribocorrosion) on the surface degradation of the said materials.

Wieczorek [69] examined ADI under a combined impact of dynamic forces and abrasive grains, only to conclude that under such conditions, the surface wear of the elements subject to tests increased compared to the wear in the presence of the abrasive material alone, and demonstrated the synergy of the effects caused by both degradation factors. Navarro-Mesa et al. [70] studied the tribological properties of austempered grey irons (AGI) by pin-on-disc testing in dry and wet environments. Under dry conditions, the wear resistance of AGIs increased as the austempering temperature dropped, while the wear resistance of AGIs under humid conditions increased along with the austempering temperature rise. Stachowiak and Wieczorek [71] analysed the combined effect of corrosive action (water + 3.5% NaCl) and wear on the tribocorrosion of ADI, and concluded that the increase

in abrasion resistance and hardness were correlated. However, the highest surface hardness did not entail the highest resistance to tribocorrosion. The lowest tribocorrosion wear was found in the case of the cast iron characterised by an austenite content of ca. 20% and a hardness of 382 HB. Having studied the hardest cast iron variant, it was established that the increased wear, compared to the cast iron variants of lower hardness, could be attributed to intense corrosion processes initiated where cracks emerged in the hard surface layer.

In industrial practice, especially mining, one typically deals with a combined effect of an abrasive material, a corrosive agent (water), and variable impact loading. Such a form of degradation is referred to further on in this paper as impact–abrasion–corrosion wear. Unlike impact–abrasion and tribocorrosion, multifactorial wear is a process which has been explored to a relatively limited extent, hence the need for further research in this field. At the current stage of development, the literature on the subject addressed in this paper contains no results of studies of multifactorial wear, especially with regard to the combined effect of degradation factors such as abrasive material, water, and pulse excitation, concerning ADI. In that respect, this paper will represent a novelty, given the state of the art.

The main purpose of the studies addressed in this article was to become familiar with the wear characteristics of ausferritic cast irons under the conditions of multifactorial wear, and the following problems were taken into consideration in particular:

- Effect of the content of retained austenite on multifactorial wear, including impact–abrasion–corrosion;
- Relationship between multifactorial wear and service hardness of the surface layer.

The studies in question were conducted at a dedicated test rig enabling one-, two- and three-factor wear to be generated.

2. Materials and Methods

2.1. Research Method

The research aimed at establishing the properties of ADI with diversified structure under multifactorial wear conditions was broken down into three stages.

Stage 1 comprised determination of the initial post-austempering structure of the chain drums subject to the tests, as well as the hardness and austenite content of this structure. Additionally, parameters characterising the susceptibility of the materials examined to corrosion were identified (detailed characteristics of the test chain drums are described in Section 2.2).

The structure of the ductile irons in questions was determined by studying the reference chain drums and by out samples from the zone of mating between the seat and the chain link. The samples were then ground, polished, and etched in a 2% Nital solution. Next, the polished surfaces were etched and subjected to metallographic observations at magnifications of $\times 50 \div 1000$ using the OLYMPUS IX70 light microscope (Olympus Company, Tokyo, Japan). Hardness measurements were conducted in the drum cross-section, including in the seat/chain mating zone, by applying the Brinell method.

The austenite fraction in the cast irons subject to the studies was determined by phase composition tests, performed using the X'Pert PRO X-ray diffractometer from Panalytical, (Malvern Panalytical Ltd, Malvern, UK) featuring a cobalt anode X-ray tube ($\lambda K\alpha = 0.179$ nm) and a PIXcel 3D detector. Diffractograms were recorded in the Bragg–Brentano geometry within the angle range of $5\text{--}100^\circ 2\Theta$, with a step of 0.026° and a counting time of 80 s per step. A qualitative X-ray phase analysis was performed using the HighScore Plus software (v. 3.0e) and the PAN-ICSD database of inorganic crystal structures.

In Stage 2, wear tests were conducted using a dedicated test rig that made it possible to generate conditions in which an electrochemical corrosion-promoting agent, abrasion, and dynamic excitation exerted a combined effect. Tests were also performed in the presence of the quartz sand mineral abrasive alone, as well as by applying a combination of two factors: abrasive material along with dynamic excitation, and abrasive material with water. Table 1 contains a summary of the variants tested for the effect of the degradation factors. Also at

this stage, wear characterising measures were determined for all the impact variants of the degradation factors (the test rig, the test method, and the method employed to determine the wear measures are described in Section 2.3).

Table 1. Combinations of the damaging agents.

Research Variant and Its Designation	Destructive Factors	Simulated Type of Wear
Variant A	quartz sand	abrasive wear
Variant AD	quartz sand and dynamic force	abrasive–dynamic wear
Variant AC	quartz sand and water	tribocorrosion wear
Variant ACD	quartz sand, water and dynamic force	abrasive–corrosion–dynamic wear

The last stage of the research comprised determining the post-wear test structure of the ductile irons, analysing the surface damage mechanisms, and measuring hardness by the Brinell method. The related tests were performed in a cross-section through the chain drum seat and chain link mating zone (Figure 2).

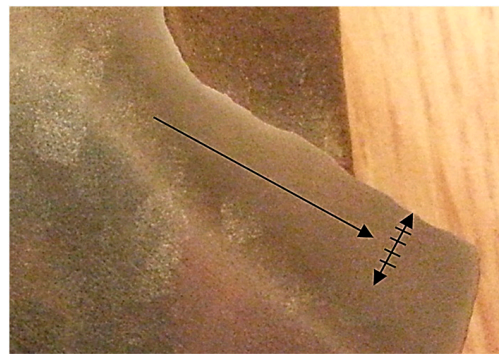


Figure 2. Zone of the test chain drum subject to microscopic observations; the arrow indicates the hardness measurement range.

2.2. Object of Research

The collective object of the research was chain wheels (Figure 3) manufactured from ductile iron and heat-treated. The chemical composition and heat treatment parameters were determined on the basis of previous studies [16,47,68] and their compliance with anti-wear requirements was confirmed based on tests under real conditions. The area subject to wear was the zone of mating between the chain drum and chain links.

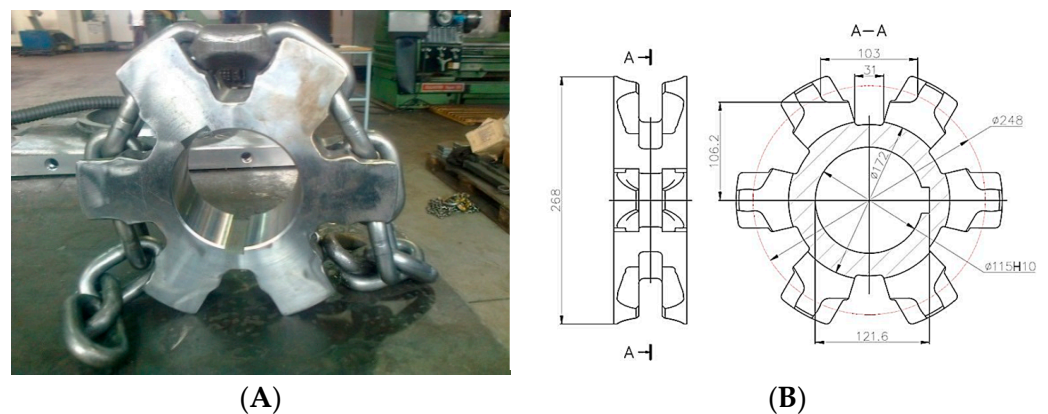


Figure 3. Chain drum subject to tests: (A) view of the chain drum; (B) drum dimensions.

Four sets of chain drums were studied (each drum tested under only one variant of the combination of degradation factors), and all of them were manufactured from the same austempered ductile iron (its chemical composition is provided in Table 2). The ductile iron was compliant with the applicable standard [72], and it was characterised by a pearlite–ferrite structure, the number of graphite nodules of 200/mm², and nodularity greater than 90%. The test drums were cast using sand moulds. After the casting was completed, the surface of the drums was cleaned and the metal from the sprue and risers was cut off, followed by salt austempering. The thermal parameters of the heat treatment procedure applied are collated in Table 3. Following the heat treatment, the basic mechanical properties of the ductile irons studied were determined (Table 4).

Table 2. Chemical composition of ductile iron [mass%].

C	Si	Mn	S	P	Mg	Cr	Cu	Ni	Mo
3.50	2.54	0.16	0.013	0.041	0.047	0.026	0.50	1.40	0.24

Table 3. The process parameters used for manufacturing the tested ADI.

Heat Treatment Parameter	ADI_1400	ADI_1200	ADI_1000	ADI_800
Austenitising temperature, °C			950	
Austenitising time, min			180	
Austempering temperature, °C	240	270	310	360
Austempering time, min			150	

Table 4. Mechanical properties of the tested ADI.

Mechanical Property	ADI_1400	ADI_1200	ADI_1000	ADI_800
Tensile Strength TS, MPa	1507	1372	1132	1028
Yield Strength YS, MPa	1072	936	804	652
Impact Toughness K, J	54	72	84	124
Elongation A5, %	3	4	5	10

2.3. Wear Testing Station

The wear properties of the alloyed ductile irons in question were studied at a test rig which made it possible to alter the combined effect of the degradation factors affecting the drums subject to testing. The test rig is shown in Figure 4. It has been described in detail in paper [73].

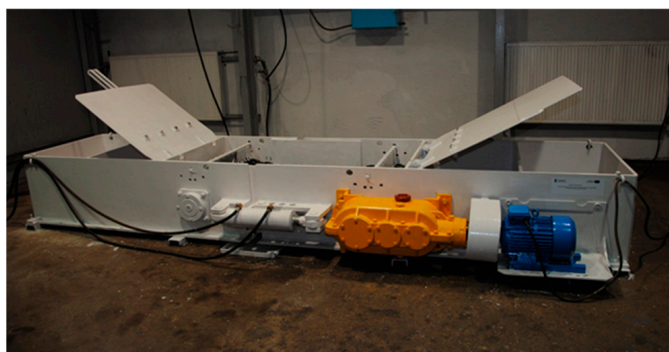


Figure 4. Test rig.

The abrasive wear of the chain drums subject to tests was induced by pouring rinsed quartz sand of a grain size smaller than 1 mm into the test rig's container. As a consequence of the chain movement, the mating zone between the chain wheels studied and the chain

surface was filled at the very beginning of the tests (chain links with the dimensions of $\varnothing 18 \times 64$ were used in the tests). Tribocorrosion was induced similarly to abrasive wear, the exception being that tap water of the composition specified in Table 5 was added to the quartz sand. The initial water-to-quartz abrasive proportion was 10%, while on the account of the observed increase in the temperature of the abrasive mixture, water was added to the mixture every 2 h in the amount of 20 L during the test rig operation. Dynamic excitation was produced by means of one-kilogramme beaters hitting tooth crests as the drum was rotating.

Table 5. Chemical composition of the water used in the tests.

Parameter	Value
Ammonium ion (NH ₄ ⁺)	<0.05 mg/dm ³
Nitrites (NH ₂ ⁻)	<0.03 mg/dm ³
Manganese (Mn)	<4.0 mg/dm ³
Iron (Fe)	<60.0 mg/dm ³
pH	7.2

The chain drums were tested under the following conditions:

- Peripheral velocity of chain drums: 0.7 m/s;
- Total test duration: 200 h (100 h for each direction of motor rotation);
- Pressure on surface between drum seat and chain link: 48.9 MPa.

The chain drum parameters were measured using a coordinate measuring machine (CMM) before and after wear testing, along a pre-established measuring path covering the drum seat and chain link mating zone. The measurements delivered coordinates of a given measuring point before and after the wear effect, and then the $\delta_{i,N}$ distance between them was determined according to the following formula:

$$\delta_{i,N} = \frac{\sqrt{(x_{1i,N} - x_{2i,N})^2 + (y_{1i,N} - y_{2i,N})^2 + (z_{1i,N} - z_{2i,N})^2}}{n} \quad (1)$$

where $x_{1i,N}$ is the x coordinate for the i th point of the N th tooth before the wear test, $x_{2i,N}$ is the x coordinate for the i th point of the N th tooth after the wear test, $y_{1i,N}$ is the y coordinate for the i th point of the N th tooth before the wear test, $y_{2i,N}$ is the y coordinate for the i th point of the N th tooth after the wear test, $z_{1i,N}$ is the z coordinate for the i th point of the N th tooth before the wear test, $z_{2i,N}$ is the z coordinate for the i th point of the N th tooth after the wear test, N is the tooth seat's numerical designation, and n is the number of seat surfaces of a given chain wheel ($n = 24$).

The procedure described above was followed to establish an averaged wear behaviour along the measuring path, which made it possible to compare the wear of the drums subject to tests under different conditions. Furthermore, a single-number wear index of δ_{MAX} was determined in the following form:

3. Results

3.1. Identification of the Initial Structure of ADI and Its Corrosion Properties

Having studied the microstructure of the ADI austempered at the temperatures of 360 °C (ADI_800) and 310 °C (ADI_1000), an upper ausferrite composed of bainitic ferrite and austenite was found in the matrix structure (Figure 5A,B), and additionally, block austenite was detected in areas between the ausferrite packets. The matrix structure of ADI_270 and ADI_240 (Figure 5C,D) was lower ausferrite, composed of ferrite, trace amounts of martensite, and low-carbon austenite. In all the materials examined, nodular graphite, typical of ductile irons, was found.

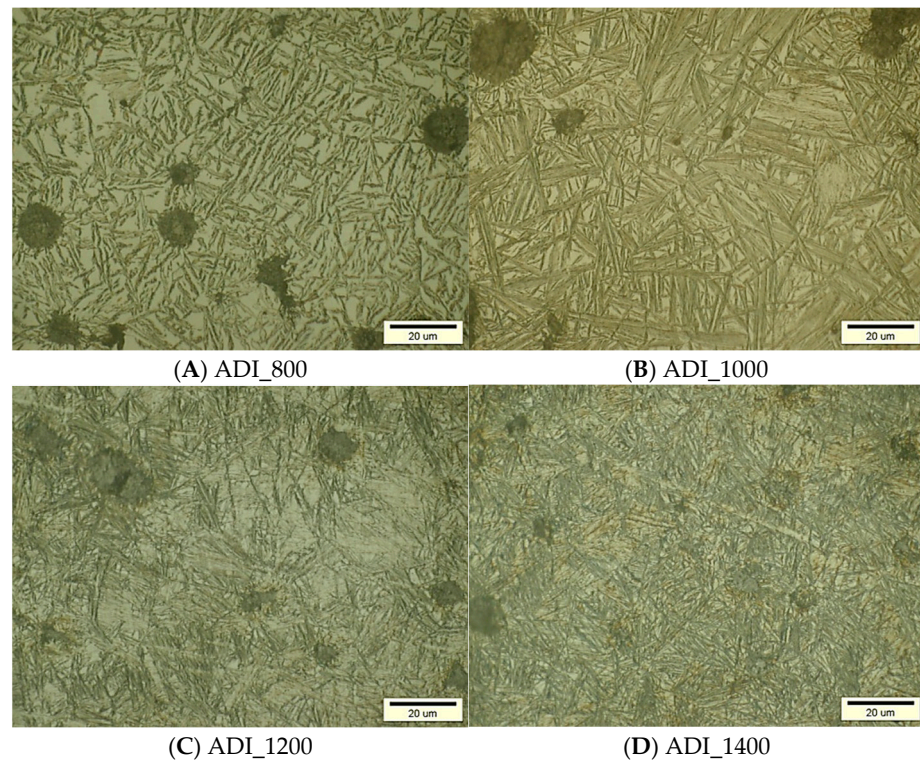


Figure 5. Microstructure of the ductile iron variants tested, 1 mm below the surface: (A–D)—(LM, $\times 1000$ magnification).

Figure 6 illustrates the results delivered by the diffractometry of the ductile irons in question, based on which the fraction of the ferrite and austenite phases in the matrix was determined. The results provided in Table 6 clearly imply that as the austempering temperature increases, so does the austenite content (the result being consistent with the findings of other researchers, e.g., those provided in [57,59]).

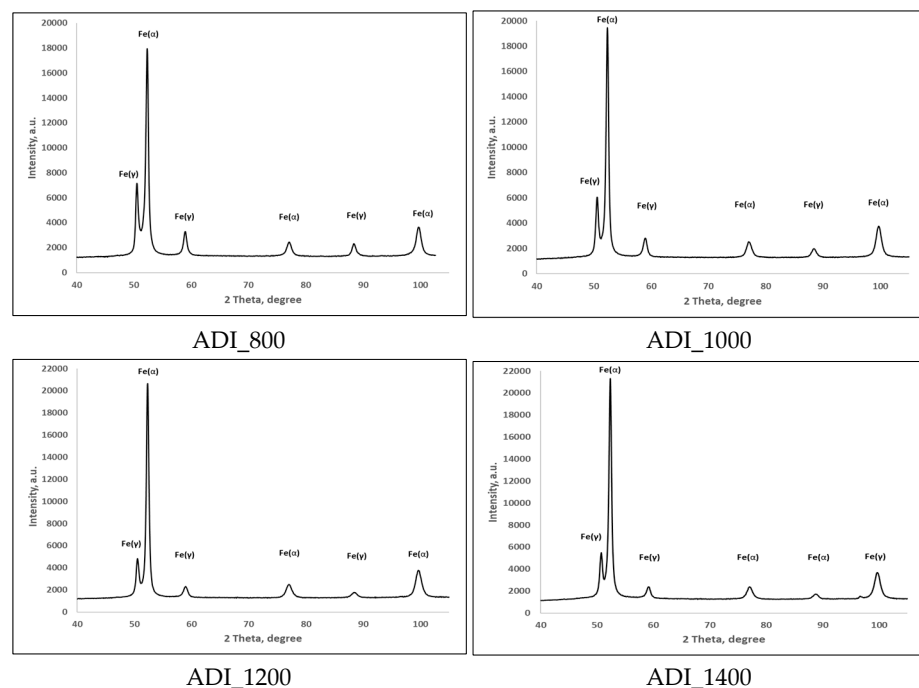


Figure 6. Diffraction profiles of the ADI variants tested; Fe(α)—ferrite, Fe(γ)—austenite.

Table 6. Fractions of individual phases in the matrix of the tested ADI.

Fractions of Individual Phases	ADI_1400	ADI_1200	ADI_1000	ADI_800
α	82.1 ± 2.5	75.4 ± 1.7	69.1 ± 1.5	59.3 ± 1.4
γ	17.9 ± 0.7	24.6 ± 1.9	30.9 ± 1.2	40.7 ± 2.5

In order to determine the susceptibility of the ductile irons studied to corrosion, a 3.5% NaCl solution was used to measure the corrosion potential (E_{corr}) and corrosion current density (i_{corr}) by the Tafel method. The results obtained are provided in Table 7. The differences found in the corrosion current density values for the tested variants of ductile cast iron are relatively small and close to the standard deviation. It can therefore be concluded that the matrix of the tested cast irons does not significantly affect their resistance to the corrosive effects of a solution of water and 3.5% NaCl.

Table 7. Values of corrosion potential (E_{corr}) and corrosion current density (i_{corr}) measured for the ADI tested, and the corrosion rates (W_{corr}) established on such a basis, corresponding to a wear test time of 200 h.

Parameter	ADI_800	ADI_1000	ADI_1200	ADI_1400
E_{corr} , mV (SCE)	-590 ± 15	-501 ± 16	-493 ± 12	-676 ± 16
i_{corr} , $\mu\text{A}/\text{cm}^2$	16.1 ± 2.1	13.8 ± 1.5	12.4 ± 1.8	14.8 ± 2.1
W_{CORR}	0.0041 ± 0.0001	0.0041 ± 0.0001	0.0044 ± 0.0009	0.0048 ± 0.0001

3.2. Wear Test Results

After the wear tests were conducted in line with the method specified in Section 2.3, the $\delta_{i,N}$ parameters were determined, making it possible to establish the behaviour of this parameter in a function of the position on the measuring route for the wear factor combination variants taken into consideration (Figure 7). Figure 7 clearly shows that the depth of the wear zone in the wheel seat and chain link mating area increases significantly as the number of the combined environmental factors does so. The greatest wear of the wheel surface was observed for the ACD variant, i.e., the combined effect of quartz sand, water, and dynamic excitations.

Based on the values obtained for the $\delta_{i,N}$ parameter, the maximum value (δ_{MAX}) was established for individual wear variants (Table 8). Besides the measures of wear, the behaviour of hardness of the surfaces subject to tests was also determined following the bench tests. Table 9 summarises the HB hardness values obtained in a tooth cross-section through the mating zone, 0.3 mm below the surface. The values provided in the table imply a significant hardness increase following the wear test, as observed in all the ADIs tested. Both the wear results and the surface hardness values are analysed in Section 4.

Table 8. Values of the δ_{MAX} parameter obtained for the ADIs tested.

Grade of Cast Iron	$\delta_{\text{MAX, A}}$ (Variant A)	$\delta_{\text{MAX, AD}}$ (Variant AD)	$\delta_{\text{MAX, AC}}$ (Variant AC)	$\delta_{\text{MAX, ACD}}$ (Variant ACD)
ADI_1400	0.707 ± 0.080	0.993 ± 0.137	1.096 ± 0.254	1.471 ± 0.089
ADI_1200	0.801 ± 0.079	0.914 ± 0.130	1.037 ± 0.159	1.511 ± 0.125
ADI_1000	0.920 ± 0.079	0.886 ± 0.118	0.926 ± 0.206	1.672 ± 0.158
ADI_800	0.930 ± 0.123	0.783 ± 0.097	1.033 ± 0.144	1.678 ± 0.114

Table 9. Comparison of the values of service hardness of the surface layer in the ADIs analysed following the wear tests.

HB	Initial State	Variant A	Variant AD	Variant AC	Variant ACD
ADI_1400	387 ± 5	618 ± 7	576 ± 9	618 ± 7	538 ± 6
ADI_1200	382 ± 4	600 ± 9	499 ± 7	543 ± 8	602 ± 7
ADI_1000	335 ± 3	478 ± 6	399 ± 5	441 ± 6	441 ± 6
ADI_800	284 ± 3	441 ± 6	385 ± 5	364 ± 5	377 ± 5

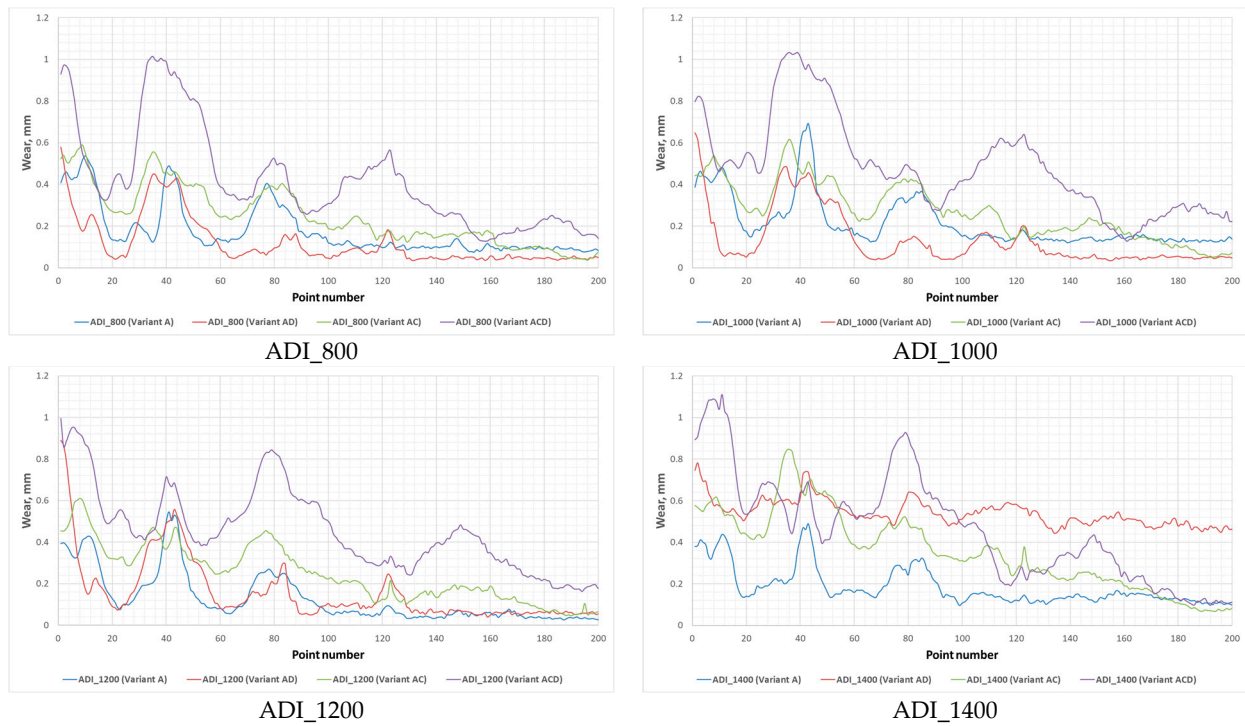


Figure 7. Curves of the $\delta_{i,N}$ wear measure, as determined for the degradation factor variants analysed.

3.3. Damage Identification in the ADIs Subjected to Tests

A single predominant damage mechanism—namely micro-scratching—was observed on the surface of the chain wheels made of ADIs following the abrasive wear tests (Variant A) (an example of the damage to the surface of ductile iron ADI_800 is shown in Figure 8A). This form of surface damage was caused by the quartz abrasive grains. The microstructure studies of the surface layer in all types of the ADI in question revealed no surface cracks; however, it was noted that, as the hardness of the ductile iron matrix decreased (thereby increasing the material's plasticity), more intense friction-induced deformations of graphite occurred at the surface, which can intensify the process of surface micro-scratching by making it easier for the irregularities of the abrasive grain to penetrate the surface layer. The foregoing relationship was particularly evident in ductile irons ADI_800 (Figure 8B) and ADI_1000.

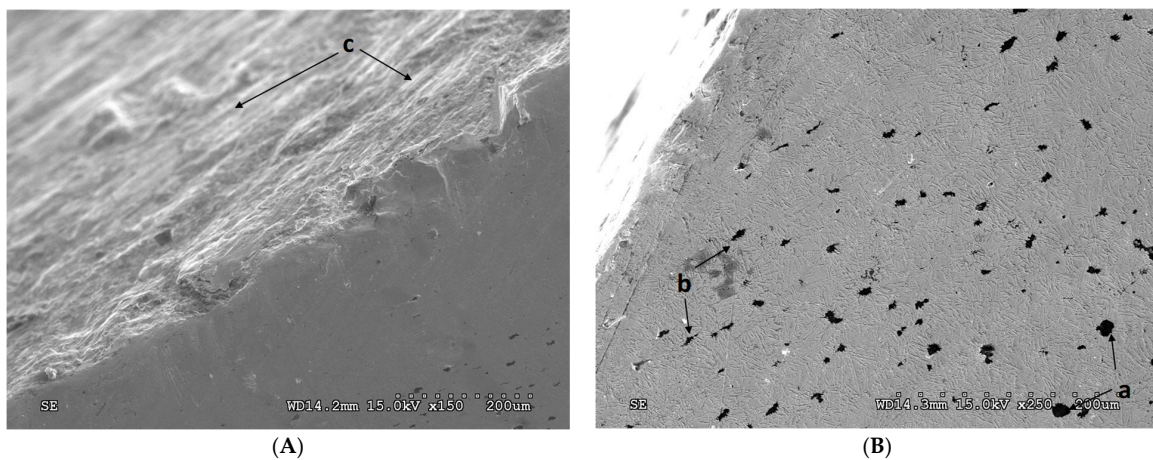


Figure 8. Examples of damage to the surface (A) and the surface layer cross-section (B) in ductile iron ADI_800 following the abrasive wear test (Variant A); a—non-deformed graphite, b—highly deformed graphite of lenticular shape, c—micro-scratch.

In the case of the combined effect of abrasive material and dynamic forces (Variant AD), the type of the damage mechanisms observed basically depended on the cast iron microstructure, and primarily on the austenite content. What could be found in the cast irons with an upper ausferrite structure and the austenite content ranging from 27 to 40% (ADI_800 and ADI_1000) was identical forms of damage as in the case of abrasive wear, the only difference being that the surface layer area with graphite deformation was smaller; moreover, no surface cracks were observed.

In the case of the ductile irons with a lower ausferrite structure (ADI_1200 and ADI_1400), as shown in Figure 9, the damage forms observed besides the micro-scratching typical of abrasion were those caused by impulse forces, i.e., cracks initiating at the surface and penetrating deep into the surface layer, matrix cracks located near discontinuities (and next to deformed graphite nodules in particular), as well as flat surface chipping.

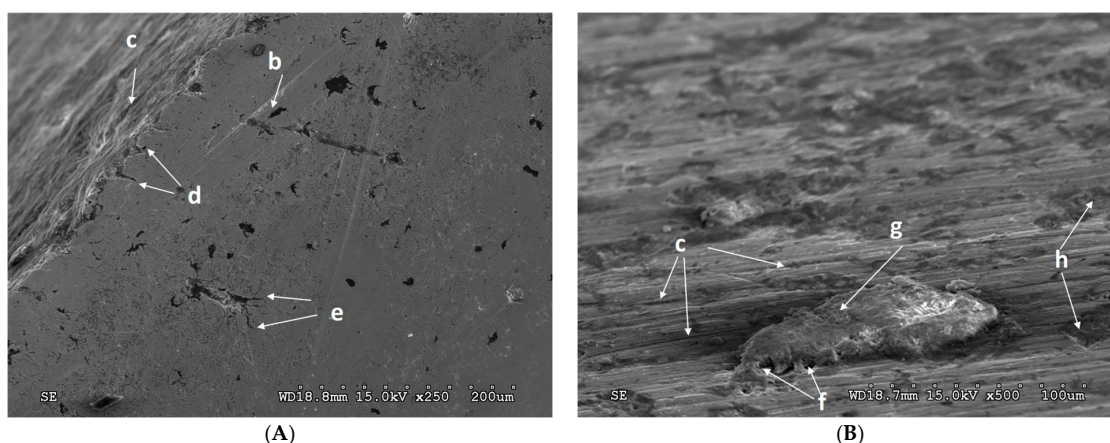


Figure 9. Surface layer (A) and examples of surface damage (B) in ductile iron ADI_1400 after testing under abrasive–dynamic wear conditions (Variant AD); b—strongly deformed lenticular graphite; c—micro-scratch; d—sub-surface cracks; e—cracks in the cast iron matrix; f—surface cracks; g—loosened surface material fragment; h—flat surface chipping; SEM.

Where the effect of the abrasive material and the corrosive agent (Variant AC) was combined, the forms of damage observed in the material were very similar to those caused by the abrasive grains alone (Variant A). This being the case, the surface degradation was also attributable to micro-scratching, and only the depth of the resulting scratches was greater (Figure 10). More intense surface material separation was promoted by the corrosion process, which was responsible for the formation of corrosion wear products (oxides of the metals contained in the cast iron) of high hardness. These oxides accelerated the micro-abrasion process in the event that they were components of the abrasive mixture; moreover, the places where they developed on the metallic surface as a result of electrochemical corrosion processes could be separated more easily by the abrasive grains.

In Variant ACD, where the surface degradation was attributable to the combined effect of the sand grain, the corrosive agent, and dynamic forces, one could observe relatively few traces of damage forms enabling a specific degradation mechanism to be identified. This was due to the high intensity of the degradation processes at play, causing the surface to be smoothed and, by that means, the typical traces of a given damage type to be removed. An example of such a smoothed surface, only with individual micro-scratches visible on the surface of ductile iron AD_1200, has been provided in Figure 11A. There are spherical or slightly deformed formations of nodular graphite visible in a cross-section through the surface layer of this ductile iron (Figure 11B).

In the case of the cast irons with a high austenite content, surface was also found to be smoothed (Figure 12A) as an effect of the degradation factors, but the nodular graphite was more deformed. Additionally, the areas of removed graphite were spotted on the surface of ductile iron ADI_800 (Figure 12B).

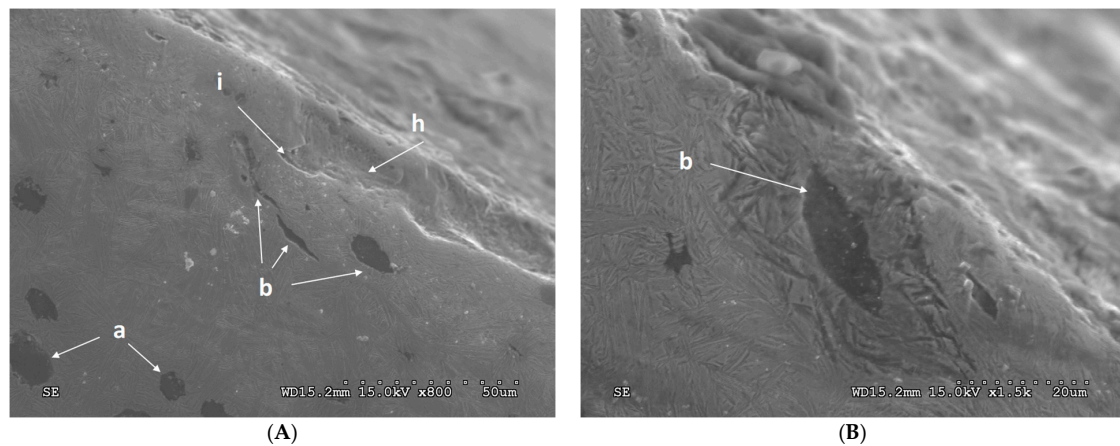


Figure 10. Surface layer (A) and friction-deformed graphite grains (B) in ductile iron ADI_800 after testing under tribocorrosion wear conditions (Variant AC); a—non-deformed graphite; b—strongly deformed lenticular graphite; h—flat surface chipping; i—area of removed graphite; SEM.

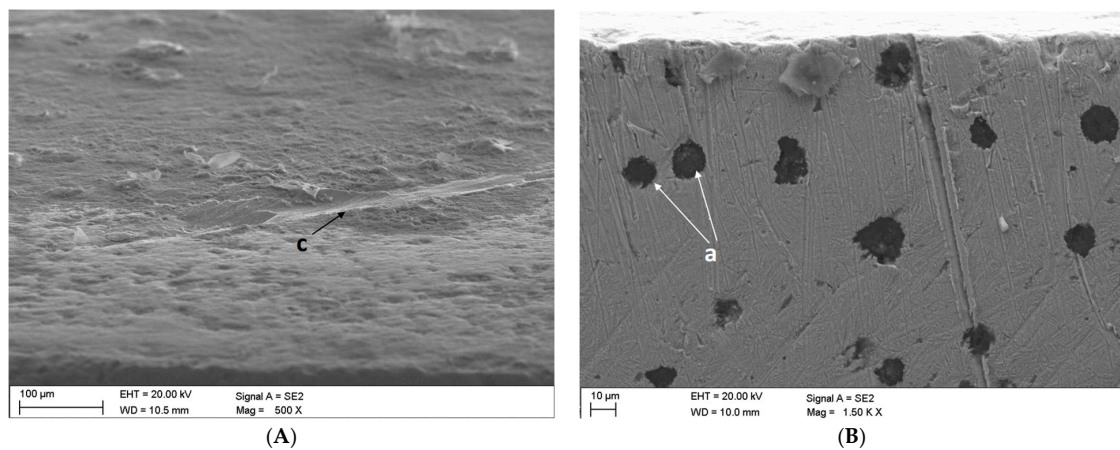


Figure 11. Examples of damage to the surface (A) and the surface layer cross-section (B) in ductile iron ADI_1200 following multifactorial wear testing (Variant ACD); a—nodular graphite; c—micro-scratch; SEM.

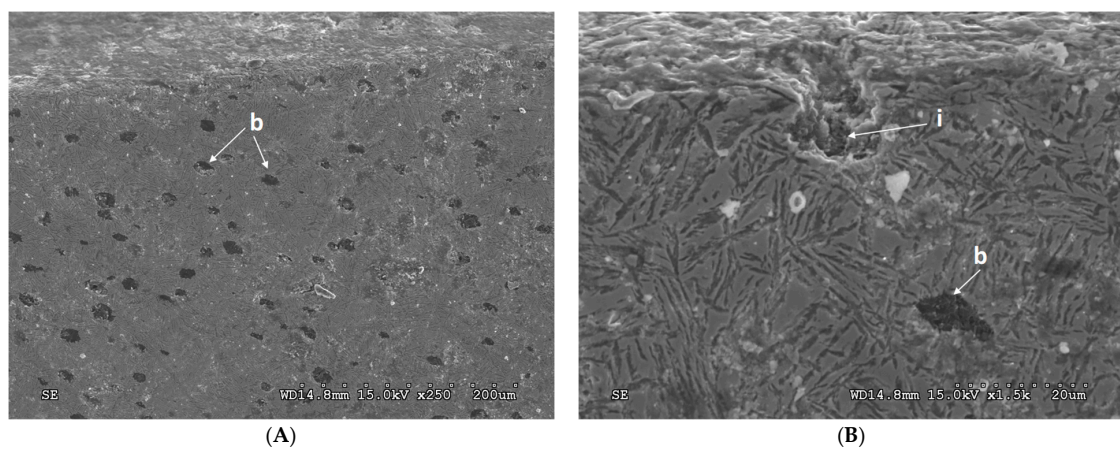


Figure 12. Surface layer (A) and forms of surface damage (B) to ductile iron ADI_800 following multifactorial wear testing (Variant AC); b—heavily deformed lenticular graphite; i—area of removed graphite; SEM.

However, having examined the cross-sections through the surface layer of the ductile irons with a lower ausferrite matrix (ADI_1200 and ADI_1400), it was found to be cracking, particularly in the lower zone of surface chipping (Figure 13A) and in the areas of removed graphite (Figure 13B). These damage forms were relatively rare considering the entire surface subject to wear, yet their effects were significant.

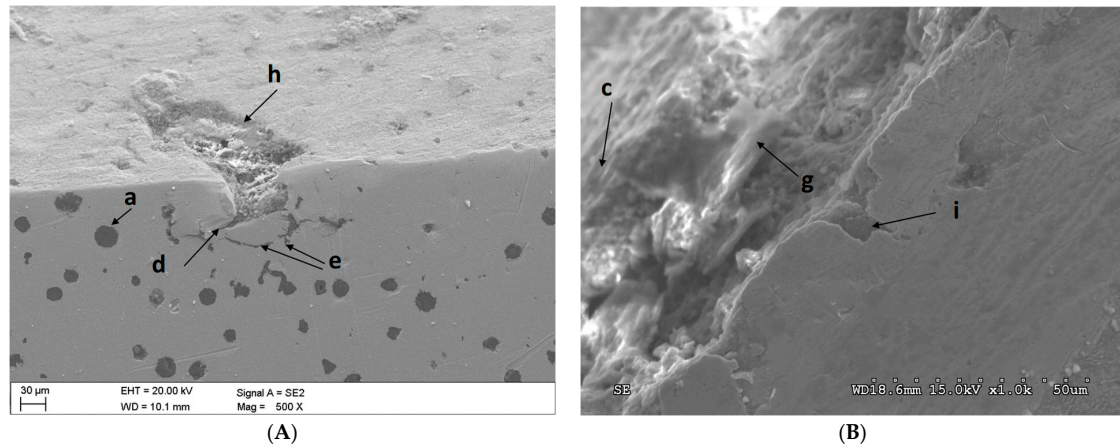


Figure 13. Cracks in the surface layer of ductile irons ADI_1200 (A) and ADI_1400 (B) following multifactorial wear testing (Variant ACD); a—non-deformed graphite; c—micro-scratch; d—sub-surface cracks; e—cracks in the cast iron matrix; g—loosened surface fragment; h—flat surface chipping; i—area of removed graphite with visible cracks; SEM.

4. Discussion

The analysis of the surface damage observed following wear testing under varying environmental conditions revealed that the occurrence of individual forms of damage is heavily affected by the matrix microstructure, and the austenite content in particular. Therefore, further discussion of the results obtained in the studies has been functionally related to this phase component.

Figure 14 illustrates the behaviour of the δ_{MAX} wear parameter in a function of austenite content in the matrix of the ductile irons studied, as determined for the variants of the combined degradation factor effect taken into consideration.

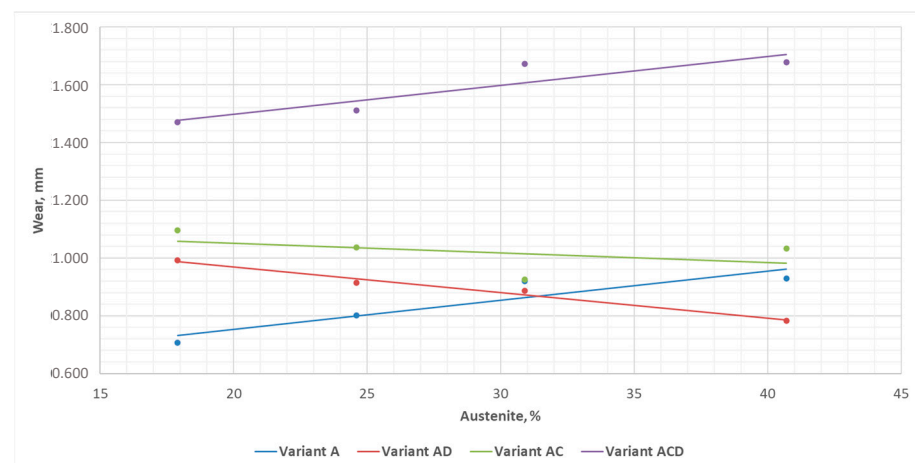


Figure 14. Values of the δ_{MAX} wear parameter in a function of austenite content in the matrix of the ductile irons tested, established for the analysed variants of the degradation factor effect combination.

The figure clearly demonstrates the progressive nature of the wear values in a function of the austenite content in the ADI matrix for the variants of abrasive wear (Variant A) and

multifactorial wear (Variant ACD). A different, degressive nature is observed in the case of impact–abrasion wear, while in the case of tribocorrosion, there is an extremum (minimum) for values of approx. 30% of austenite (which corresponds to the ADI_1200 variant). With reference to Figure 14, one can also generally conclude that, as the number of degradation factors increases, the value of wear of the chain wheels made of ADI rises as well. What may be perceived as a departure from this rule is the relatively low wear values obtained for Variant AD observed for the ductile irons with high austenite content (ADI_800 and ADI_1000). An additional observation made with regard to the aforementioned grades of cast iron is that a lenticular deformation of graphite, arranged diagonally to the surface, emerges under the impact of friction force. Such an arrangement of graphite may facilitate the abrasion of the matrix by the abrasive grains, enabling them to penetrate deeper into the surface layer.

The observed increase in the wear of the ADI chain wheels correlating with the increasing austenite content in their microstructure is consistent with the research results discussed in other papers [59,64], and it generally stems from the lower technological hardness of the surface layer of cast irons with a lower austenite content (see Table 9). However, when loaded, austenite transforms into martensite of the TRIP type in ADI, which significantly alters the operating characteristics of the surface layer in these ductile irons.

Figure 15A,B shows diverse diffraction profiles of the ADI_1400 ductile iron variant, including for the initial condition of the ductile iron and following its abrasive wear testing (the XRD test parameters differed from those applied to determine the austenite content). It clearly implies that, as a result of both wear tests, compared to the initial condition, there was a decrease in the peak associated with iron γ (it is observed, for instance, for the values of angle $2\Theta \approx 41^\circ$) and an increase in the peak associated with iron α (occurring for the values of angle $2\Theta \approx 43^\circ$). The XRD test results obtained evidence the TRIP-type transition under the pressure induced by wear testing.

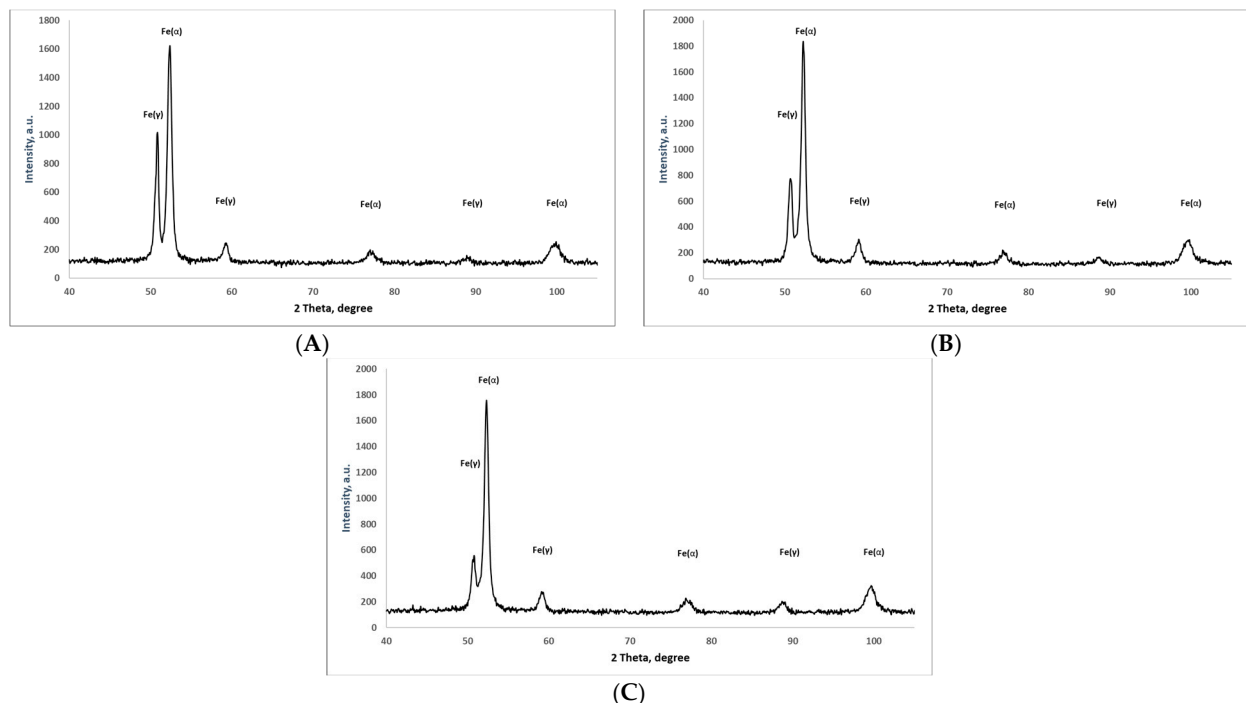


Figure 15. Diffraction profiles of the ADI_1400 ductile iron in the initial condition: (A) after abrasion testing (B) and after tribocorrosion testing. (C) Fe(α)—ferrite, Fe(γ)—austenite.

As a direct result of the austenite transition into martensite, the service hardness of the surface layer increased (Table 9), and subsequently, its wear resistance improved. By the effect of the abrasive quartz grains, the initial hardness of the ADI increased by

143–231 HB. However, as Figure 16 implies, the increase in the hardness of this layer depends, to a considerable extent, on the wear testing conditions (which is also confirmed by the information provided in Table 10, listing the values of Pearson’s r coefficient of correlation between the austenite content and the service hardness of the surface layer), and consequently on the combination of degradation factors, but also on the austenite content in the cast iron microstructure.

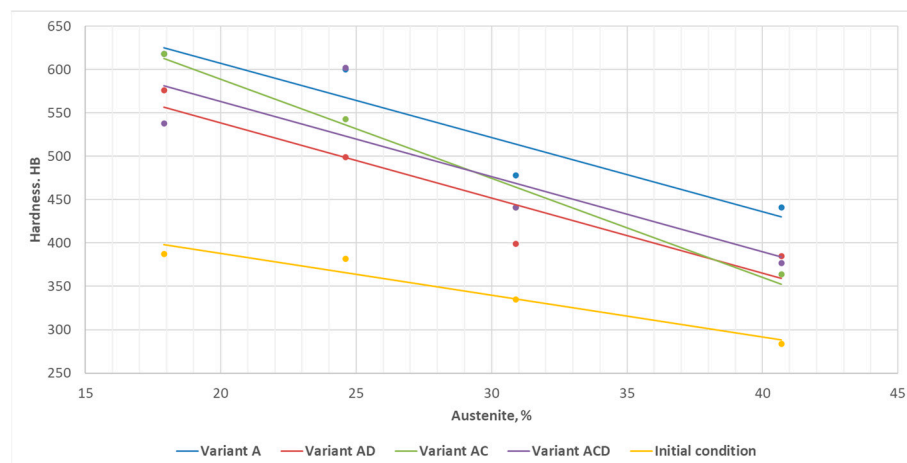


Figure 16. Curves of surface hardness in a function of austenite content in the matrix of the ductile irons subject to tests, as determined for the analysed variants of combination of the degradation factors.

Table 10. The Pearson coefficient of correlation (r) between the austenite content and the service hardness of the surface layer in ADI studied.

	Variant A	Variant AD	Variant AC	Variant ACD
r	−0.921	0.989	0.757	−0.876

To recapitulate on the foregoing, the wear decrease observed for Variant A, correlating with the decrease in the austenite content in the ADI microstructure is mainly attributable to the higher hardness of the surface layer which has developed under load.

In the case of a pulse-type abrasion, one can observe increasing wear as the austenite content decreases in the structure of ADI (Figure 14). The most favourable anti-wear properties were displayed by the ADI_800 ductile iron, the ADI_1000 material being ranked second in this respect, while the lowest resistance to this type of wear was established for the ADI_1400 material variant. At the same time, Figure 16 implies that the service hardness of the surface layer attained in Variant AD is the lowest among all the wear variants taken into consideration.

The most probable reason for the foregoing is the reduced intensity of the TRIP-type phase transition, caused by the occurrence of surface layer cracks, thereby leading to a reduction in the forces required to detach material in the course of abrasion. As argued in the papers by Putatunda and Bingi [74], Yang and Putatunda [40,41], and Ravishankar et al. [75], what happens during the TRIP-type phase transition is the formation of martensite, responsible for wear resistance enhancement, but at the same time, the resistance to brittle cracking (K_{1C}) of ADI declines as the ausferritising temperature drops, causing the austenite content in the microstructure to decrease as well. What can be concluded with reference to the test results obtained is that the chain wheels made of ADI with an upper ausferrite structure are better suited for operation under the conditions of abrasive wear and variable dynamic forces.

The behaviour of wear of ADI under the conditions of tribocorrosion in a function of austenite content (Figure 14) is generally similar in nature to that of impact–abrasion

wear; however, the slope of the regression line is smaller, which indicates certain similarity between the damage mechanisms observed for both wear forms. As aforementioned, the reason for the relationship identified with regard to impact–abrasion wear was recognised in the occurrence of cracks in the surface layer and the reduced intensity of the austenite transition into martensite. In the case of tribocorrosion wear, on the account of the absence of dynamic forces, no cracks developed in the surface layer during the tests, which was confirmed by damage analysis (Figure 10). However, the second factor taken into consideration, namely the weakening of the structure consolidation process, was undoubtedly at play. Attributable to the impact of water, the corrosion process caused the formation of hard oxide layers and facilitated their abrasion by quartz sand grains, which should have reduced the intensity of the TRIP-type process. The above finding was confirmed by the service hardness decrease compared to the abrasive wear and its increase compared to the impact–abrasion process (Table 9 and Figure 16), as well as the reduced fraction of the α phase, as observed in Figure 15 following XRD testing.

The nature of the wear behaviour observed in the multifactorial (impact–abrasion–corrosion) tests is identical to that of abrasive wear; however, the intensity of this process is higher. The combined wear processes induce intense surface micro-scratching (Figure 11), surface layer cracking (Figure 13), and considerable surface oxidation. The former of these processes should exert a progressive impact on the TRIP-type transformation, while the other two should act in a degressive manner. Ultimately, it can be noticed that the parameters of surface hardening under load are lower than those obtained following abrasive wear, while being higher than those measured after impact–abrasion testing and those attributable to tribocorrosion wear (for most of the ADI tested). The wear progression observed to be dependent on the increasing austenite content in the microstructure implies that multifactorial wear is predominantly abrasive in nature. The foregoing is attributable to a number of reasons, but primarily to the growing surface micro-abrasion effect of abrasive material under the impact of dynamic external forces, the higher accumulation of hard oxide particles in the abrasive, and the stronger synergistic effect associated with the interaction between environmental factors (the synergy of the surface layer degradation processes is not among the subjects discussed in this paper, but it will be addressed in the author’s subsequent studies).

5. Conclusions

1. Following a series of bench tests, making it possible to reproduce the processes of the wear of chain wheels made of Ni-Cu alloyed austempered ductile iron, one of the conclusions formulated in this paper, is that the combined effect of dynamic forces, corrosion, and quartz sand-based abrasives causes increased surface degradation in the cast iron grades subject to the studies compared with processes characterised by a reduced number of degradation factors (i.e., one- or two-factor wear processes).
2. The chain wheels made of ADI were found to have sustained the greatest damage under the impact–abrasion–corrosion (three-factor) wear scenario, while the wear was least advanced in the abrasion (one-factor) wear case. The two-factor wear was characterised by parameter values found to be intermediate between those obtained for the variants mentioned above, with a greater wear being observed for the tribocorrosion variant.
3. The study demonstrated an increasing service hardness of the surface layer of chain wheels made of ADI following wear processes compared to the hardness of an unworn surface of ductile irons.
4. The increase in the value of the surface layer hardness following wear tests depends on the combination of degradation factors, and the largest hardness increase has been established for the abrasive wear variant.
5. The predominant forms of surface damage are as follows:
 - For abrasion wear—micro-scratching;
 - For impact–abrasion wear—micro-scratching and matrix cracking;

- For tribocorrosion wear—micro-scratching and corrosion;
- For impact–abrasion–corrosion wear—micro-scratching and matrix cracking.

Funding: The study was carried out as a part of the project “Innovative technology for production of tension members for transport systems with the use of cast materials”, The National Centre for Research and Development, No. POIG.01.04.00-24-100/11.

Data Availability Statement: Data are contained within the article.

Conflicts of Interest: The author declares no conflicts of interest.

References

1. Gilewski, R.; Kopyciński, D.; Guzik, E.; Szczesny, A. Shaping the Microstructure of High-Aluminum Cast Iron in Terms of the Phenomenon of Spontaneous Decomposition Generated by the Presence of Aluminum Carbide. *Materials* **2021**, *14*, 5993. [[CrossRef](#)] [[PubMed](#)]
2. Wieczorek, A.N. Designing machinery and equipment in accordance with the principle of sustainable development. *Manag. Syst. Prod. Eng.* **2015**, *1*, 28–34.
3. Wang, H.; Li, Z. Safety management of coal mining process. In *IOP Conference Series: Earth and Environmental Science*; IOP Publishing: Jeju Island, Republic of Korea, 2020; p. 598.
4. Szewerda, K.; Tokarczyk, J.; Wieczorek, A. Impact of Increased Travel Speed of a Transportation Set on the Dynamic Parameters of a Mine Suspended Monorail. *Energies* **2021**, *14*, 1528. [[CrossRef](#)]
5. Angeles, E.; Kumral, M. Optimal Inspection and Preventive Maintenance Scheduling of Mining Equipment. *J. Fail. Anal. Prev.* **2020**, *20*, 1408–1416. [[CrossRef](#)]
6. Liao, X.; Zheng, Z.; Liu, T.; Long, J.; Wang, S.; Zhang, H.; Zheng, K. Achieving high impact–abrasion–corrosion resistance of high–chromium wear–resistant steel via vanadium additions. *J. Mater. Res. Technol.* **2024**, *29*, 2425–2436. [[CrossRef](#)]
7. Xia, R.; Li, B.; Wang, X.; Yang, Z.; Liu, L. Screening the Main Factors Affecting the Wear of the Scraper Conveyor Chute Using the Plackett–Burman Method. *Hindawi Math. Probl. Eng.* **2019**, *2019*, 1204091. [[CrossRef](#)]
8. Kirchgäßner, M.; Badisch, E.; Franek, F. Behaviour of iron-based hardfacing alloys under abrasion and impact. *Wear* **2008**, *265*, 772–779. [[CrossRef](#)]
9. Saha, G.; Valtonen, K.; Saastamoinen, A.; Peura, P.; Kuokkala, V.T. Impact-abrasive and abrasive wear behavior of low carbon steels with a range of hardness-toughness properties. *Wear* **2020**, *450*, 203263. [[CrossRef](#)]
10. Widder, L.; Varga, M.; Adam, K.; Kuttner, A. Development of Impact Energy Distribution of Various Abrasives during Cyclic Impact/Abrasion Testing. *Solid State Phenom.* **2017**, *267*, 234–242. [[CrossRef](#)]
11. Kennedy, D.M.; Helali, M.; Hashmi, M.S.J. Dynamic abrasion resistance of coatings applied to engineering materials. *Surf. Coat. Technol.* **1994**, *68–69*, 477–481. [[CrossRef](#)]
12. Ratia, V.; Valtonen, K.; Kuokkala, V.-T. Impact-abrasion wear of wear-resistant steels at perpendicular and tilted angles. *Proc. Inst. Mech. Eng. Part J J. Eng. Tribol.* **2013**, *227*, 868–877. [[CrossRef](#)]
13. Teeri, T.; Kuokkala, V.T.; Siitonen, P.; Kivikyto, P.; Liimatainen, J. Impact wear in mineral crushing. *Proc. Est. Acad. Sci. Eng.* **2006**, *12*, 408–418.
14. Ratia, V.; Valtonen, K.; Kemppainen, A.; Kuokkala, V.-T. High Stress Abrasion and Impact-Abrasion Testing of wear Resistant Steels. *Tribol. Online* **2013**, *8*, 152–161. [[CrossRef](#)]
15. Chintha, A.R.; Valtonen, K.; Kuokkala, V.T.; Kundu, S.; Peet, M.J.; Bhadeshia, H.K.D.H. Role of fracture toughness in impact-abrasion wear. *Wear* **2019**, *428*, 430–437. [[CrossRef](#)] [[PubMed](#)]
16. Wieczorek, A.N. Operation-oriented studies on wear properties of surface-hardened alloy cast steels used in mining in the conditions of the combined action of dynamic forces and an abrasive material. *Arch. Metall. Mater.* **2017**, *62*, 2381–2389. [[CrossRef](#)]
17. Sundström, A.; Rendón, J.; Olsson, M. Wear behaviour of some low alloyed steels under combined impact/abrasion contact conditions. *Wear* **2001**, *250*, 744–754. [[CrossRef](#)]
18. Ratia, V.; Heino, V.; Valtonen, K.; Vippola, M.; Kemppainen, A.; Siitonen, P.; Kuokkala, V.T. Effect of abrasive properties on the high-stress three-body abrasion of steels and hard metals. *Tribol.—Finn. J. Tribol.* **2014**, *32*, 3–18.
19. Wilson, R.D.; Hawk, J.A. Impeller wear impact-abrasive wear test. *Wear* **1999**, *225*, 1248–1257. [[CrossRef](#)]
20. Mindivan, F.; Yildirim, M.P.; Bayindir, F.; Mindivan, H. Corrosion and Tribocorrosion Behavior of Cast and Machine Milled Co-Cr Alloys for Biomedical Applications. *Acta Phys. Pol.* **2016**, *129*, 701–704. [[CrossRef](#)]
21. Mischler, S. Triboelectrochemical techniques and interpretation methods in tribocorrosion: A comparative evaluation. *Tribol. Int.* **2008**, *41*, 573–583. [[CrossRef](#)]
22. Watson, S.W.; Friedersdorf, F.J.; Madsen, B.W.; Cramer, S.D. Methods of measuring wear-corrosion synergism. *Wear* **1995**, *181–183*, 476–484.
23. Jemmely, P.; Mischler, S.; Landolt, D. Electrochemical modeling of passivation phenomena in tribocorrosion. *Wear* **2000**, *237*, 63–76. [[CrossRef](#)]

24. Cao, S.; Mischler, S. Modeling tribocorrosion of passive metals—A review. *Curr. Opin. Solid State Mater. Sci.* **2018**, *22*, 127–141. [[CrossRef](#)]
25. Ponthiaux, P.; Wenger, F.; Celis, J.P. Tribocorrosion: Material behaviour under combined conditions of corrosion and mechanical loading. In *Corrosion Resistance*; Books on Demand GmbH: Norderstedt, Germany, 2012.
26. Bailey, R.; Sun, Y. Corrosive-Wear Performance of Grade 316 Stainless Steel Sliding Against Grade 316 Stainless Steel in NaCl Solution. *J. Mater. Eng. Perform.* **2023**, 1–13. [[CrossRef](#)]
27. Dalmau, A.; Richard, C.; Igual-Muñoz, A. Degradation mechanisms in martensitic stainless steels: Wear, corrosion and tribocorrosion appraisal. *Tribol. Int.* **2018**, *121*, 167–179. [[CrossRef](#)]
28. Ghanbarzadeh, A.; Salehi, F.M.; Bryant, M.; Neville, A. A New Asperity-Scale Mechanistic Model of Tribocorrosive Wear: Synergistic Effects of Mechanical Wear and Corrosion. *J. Tribol.* **2019**, *141*, 021601. [[CrossRef](#)]
29. Fallahnezhad, K.; Feyzi, M.; Ghadirinejad, K.; Hashemi, R.; Taylor, M. Finite element-based simulation of tribocorrosion at the head-neck junction of hip implants. *Tribol. Int.* **2022**, *165*, 107284. [[CrossRef](#)]
30. Jiang, J.; Islam, M.A.; Xie, Y.; Stack, M.M. Some Thoughts on Modeling Abrasion-Corrosion: Wear by Hard Particles in Corrosive Environments. *J. Bio-Tribo-Corros.* **2024**, *10*, 12. [[CrossRef](#)]
31. Stachowiak, A.; Tyczewski, P.; Zwierzycki, W. The application of wear maps for analyzing the results of research into tribocorrosion. *Wear* **2016**, *352–353*, 146–154. [[CrossRef](#)]
32. Munoz, A.I.; Espallargas, N.; Mischler, S. *Tribocorrosion*; Springer: Berlin/Heidelberg, Germany, 2020.
33. Wang, X.Y.; Li, D.Y. Investigation of the synergism of wear and corrosion using an electrochemical scratch technique. *Tribol. Lett.* **2001**, *11*, 117–120. [[CrossRef](#)]
34. Bhadeshia, H.K.D.H. *Bainite in Steels*; The Institute of Materials: Cambridge, UK, 2001.
35. Caballero, F.G.; Bhadeshia, H.K.D.H. Very Strong Bainite. *Curr. Opinoin Solid State Mater. Sci.* **2004**, *8*, 251–257. [[CrossRef](#)]
36. Hayrynen, K.L.; Keough, J.R.; Pioszak, G.L. Designing with Austempered Ductile Iron. *AFS Trans.* **2010**, *129*, 1–15.
37. Myszka, D. Cast Iron-Based Alloys. In *High-Performance Ferrous Alloys*; Rana, R., Ed.; Springer: Berlin/Heidelberg, Germany, 2020; pp. 153–210.
38. Massone, J.; Boeri, R.; Sikora, J. Production of ADI by hot shake out—Microstructure and mechanical properties. *Int. J. Cast Met. Res.* **1999**, *11*, 419–424. [[CrossRef](#)]
39. Guzik, E. ADI cast iron and its variants as modern structural alloys. In *Engineering Forum “Development of ADI Cast Iron Technology in Poland”*; Foundry Research Institute in Cracow: Cracow, Poland, 2009; pp. 37–49.
40. Yang, J.; Putatunda, S.K. Effect of microstructure on abrasion wear behavior of austempered ductile cast iron (ADI) processed by a novel two-step austempering process. *Mater. Sci. Eng. A* **2005**, *406*, 217–228. [[CrossRef](#)]
41. Yang, J.; Putatunda, S.K. Influence of a novel two-step austempering process on the strain-hardening behaviour of austempered ductile cast iron (ADI). *Mater. Sci. Eng. A* **2004**, *382*, 265–279. [[CrossRef](#)]
42. Azevedo, C.R.F.; Garboggini, A.A.; Tschipitschin, A.P. Effect of austenite grain refinement on morphology of product of bainitic reaction in austempered ductile iron. *Mater. Sci. Technol.* **1993**, *9*, 705–710. [[CrossRef](#)]
43. Ghasemi, R.; Hassan, I.; Ghorbani, A.; Dioszegi, A. Austempered compacted graphite iron—Influence of austempering temperature and time on microstructural and mechanical properties. *Mater. Sci. Eng. A* **2019**, *767*, 138434. [[CrossRef](#)]
44. Bayati, H.; Elliot, R. The concept of an austempered heat treatment processing window. *Int. J. Cast Met. Res.* **1999**, *11*, 413–417. [[CrossRef](#)]
45. Colin-García, E.; Cruz-Ramírez, A.; Romero-Serrano, J.A.; Sánchez-Alvarado, R.G.; Gutiérrez-Pérez, V.H.; Reyes-Castellanos, G. Nodule count effect on microstructure and mechanical properties of hypo-eutectic adi alloyed with nickel. *J. Min. Metall. Sect. B-Metall.* **2021**, *57*, 115–124. [[CrossRef](#)]
46. Myszka, D.; Cybula, L.; Wiczorek, A.N. Influence of heat treatment conditions on microstructure and mechanical properties of austempered ductile iron after dynamic deformation test. *Arch. Metall. Mater.* **2014**, *59*, 1181–1189. [[CrossRef](#)]
47. Wiczorek, A.N. Influence of Shot Peening on Abrasion Wear in Real Conditions of Ni-Cu-Ausferritic Ductile Iron. *Arch. Metall. Mater.* **2016**, *61*, 1985–1990. [[CrossRef](#)]
48. Zammit, A.; Abela, S.; Wagner, L.; Mhaede, M.; Grech, M. Tribological behavior of shot peened Cu-Ni austempered ductile iron. *Wear* **2013**, *302*, 829–836. [[CrossRef](#)]
49. Zammit, A.; Bonnici, M.; Mhaede, M.; Wan, R.; Wagner, L. Shot peening of austempered ductile iron gears. *Surf. Eng.* **2017**, *33*, 679–686. [[CrossRef](#)]
50. Zammit, A.; Mhaede, M.; Grech, M.; Abela, S.; Wagner, L. Influence of shot peening on the fatigue life of Cu-Ni austempered ductile iron. *Mater. Sci. Eng. A* **2012**, *545*, 78–85. [[CrossRef](#)]
51. Sevillano, J.G.; Aldazabal, J. Ductilization of nanocrystalline materials for structural applications. *Sci. Mater.* **2004**, *51*, 795–800. [[CrossRef](#)]
52. Rementeria, R.; Aranda, M.M.; Garcia-Mateo, C.; Caballero, F.G. Improving wear resistance of steels through nanocrystalline structures obtained by bainitic transformation. *Mater. Sci. Technol.* **2016**, *32*, 308–312. [[CrossRef](#)]
53. Myszka, D.; Skołek, E.; Wiczorek, A. Manufacture of toothed elements in nanoausferritic ductile iron. *Arch. Metall. Mater.* **2014**, *59*, 1227–1231. [[CrossRef](#)]
54. Myszka, D.; Wasiluk, K.; Skołek, E.; Swiatnicki, W. Nanoausferritic matrix of ductile iron. *Mater. Sci. Technol.* **2015**, *31*, 829–834. [[CrossRef](#)]

55. Panneerselvam, S. Development of Nanostructured Austempered Ductile Cast Iron. Ph.D. Thesis, Wayne State University, Detroit, MI, USA, 2017; p. 1856. Available online: https://digitalcommons.wayne.edu/oa_dissertations/1856 (accessed on 20 February 2023).
56. Myszka, D. Technological aspects of deformation-induced transformation in austempered ductile iron. In *Scientific Works of the Warsaw University of Technology. Mechanics*; Warsaw University of Technology: Warsaw, Poland, 2014.
57. Soliman, M.; Palkowski, H.; Nofal, A. Multiphase ausformed austempered ductile iron. *Arch. Metall. Mater.* **2017**, *62*, 1493–1498. [[CrossRef](#)]
58. Myszka, D. Austenite-martensite transformation in austempered ductile iron, *Arch. Metall. Mater.* **2007**, *52*, 475–480.
59. Nili-Ahmadabadi, M.; Shirazi, H. Austempered ductile cast iron: Bainitic transformation. In *Encyclopedia of Iron, Steel, and Their Alloys*; CRC Press: Boca Raton, FL, USA, 2015; pp. 217–230.
60. Ritha Kumari, U.; Prasad Rao, P. Study of wear behaviour of austempered ductile iron. *J. Mater. Sci.* **2009**, *44*, 1082–1093. [[CrossRef](#)]
61. Suchocki, C.; Myszka, D.; Wasiluk, K. Transformation Kinetics of Austempered Ductile Iron: Dilatometric Experiments and Model Parameter Evaluation. *Arch. Metall. Mater.* **2019**, *64*, 1661–1666. [[CrossRef](#)]
62. Hayrynen, K.L.; Keough, J.R. Wear Properties of Austempered Ductile Cast Irons. *AFS Trans.* **2005**, *187*, 1–10.
63. Sellamuthu, P.; Samuel, D.G.; Dinakaran, D.; Premkumar, V.P.; Li, Z.; Seetharaman, S. Austempered ductile iron (ADI): Influence of austempering temperature on microstructure, mechanical and wear properties and energy consumption. *Metals* **2018**, *8*, 53. [[CrossRef](#)]
64. Ahmadabadi, M.N.; Ghasemi, H.M.; Osia, M. Effects of successive austempering on the tribological behavior of ductile cast iron. *Wear* **1999**, *231*, 293–300. [[CrossRef](#)]
65. Chang, L.C.; Hsui, I.C.; Chen, L.H.; Lui, T.S. Effects of heat treatment on the erosion behavior of austempered ductile irons. *Wear* **2006**, *260*, 783–793. [[CrossRef](#)]
66. Myszka, D.; Wiczorek, A.N. Effect of phenomena accompanying wear in dry corundum abrasive on the properties and microstructure of austempered ductile iron with different chemical composition. *Arch. Metall. Mater.* **2015**, *60*, 483–490. [[CrossRef](#)]
67. Zhang, N.; Zhang, J.; Lu, L.; Zhang, M.; Zeng, D.; Song, Q. Wear and friction behavior of austempered ductile iron as railway wheel material. *Mater. Des.* **2016**, *89*, 815–822. [[CrossRef](#)]
68. Wiczorek, A.N. The role of operational factors in shaping of wear properties of alloyed Austempered Ductile Iron. Part I. Experimental studies abrasive wear of Austempered Ductile Iron (ADI) in the presence of loose quartz abrasive. *Arch. Metall. Mater.* **2014**, *59*, 1665–1674. [[CrossRef](#)]
69. Wiczorek, A.N. The role of operational factors in shaping of wear properties of alloyed Austempered Ductile Iron. Part II. An assessment of the cumulative effect of abrasives processes and the dynamic activity on the wear property of Ausferritic Ductile Iron. *Arch. Metall. Mater.* **2014**, *59*, 1675–1683. [[CrossRef](#)]
70. Navarro-Mesa, C.H.; Gómez-Botero, M.; Montoya-Mejía, M.; Ríos-Diez, O.; Aristizábal-Sierra, R. Wear resistance of austempered grey iron under dry and wet conditions. *J. Mater. Res. Technol.* **2022**, *21*, 4174–4183. [[CrossRef](#)]
71. Stachowiak, A.; Wiczorek, A.N. Comparative tribocorrosion tests of 30CrMo12 cast steel and ADI spheroidal cast iron. *Tribol. Int.* **2021**, *155*, 106763. [[CrossRef](#)]
72. *PN-EN 1564:2012*; Founding—Ausferritic Spheroidal Graphite Cast Irons. National Standards Authority of Ireland: Dublin, Ireland, 2012.
73. Wiczorek, A.N.; Polis, W. Operation-oriented method for testing the abrasive wear of mining chain wheels in the conditions of the combined action of destructive factors. *Manag. Syst. Prod. Eng.* **2015**, *19*, 175–178.
74. Putatunda, S.K.; Bingi, G.A. Influence of step-down austempering process on the fracture toughness of austempered ductile iron. *J. Mater. Sci. Eng. Adv. Technol.* **2005**, *5*, 39–70.
75. Ravishankar, K.S.; Rajendra Udupa, K.; Prasad Rao, P. Development of Austempered Ductile Iron for High Tensile and Fracture toughness by Two Step Austempering Process. In Proceedings of the 68th WFC—World Foundry Congress, Chennai, India, 7–11 February 2008; pp. 35–40.

Disclaimer/Publisher’s Note: The statements, opinions and data contained in all publications are solely those of the individual author(s) and contributor(s) and not of MDPI and/or the editor(s). MDPI and/or the editor(s) disclaim responsibility for any injury to people or property resulting from any ideas, methods, instructions or products referred to in the content.